Extracts of Ruta Chalepensis as Green Corrosion Inhibitor for Copper CDA 110 in 3% NaCl Medium: Experimental and Theoretical Studies

Article *in* Analytical and Bioanalytical Electrochemistry · July 2019

CITATIONS
4

READS
516

6 authors, including:

Ammouchi Nesrine
Université 20 août 1955-Skikda
12 PUBLICATIONS **161** CITATIONS
SEE PROFILE

Hamza Allal
Université Salah Boubnider Constantine 3
34 PUBLICATIONS **328** CITATIONS
SEE PROFILE

Zouaoui Emna
Université 20 août 1955-Skikda
19 PUBLICATIONS **204** CITATIONS
SEE PROFILE

Daoiya Zouied
university of 20 August 1955 University of Skikda, Algeria
7 PUBLICATIONS **62** CITATIONS
SEE PROFILE

Anal. Bioanal. Electrochem., Vol. 11, No. x, 2019, xx - yy

Proof

Analytical & Bioanalytical Electrochemistry

2019 by CEE
www.abechem.com

Full Paper

Extracts of Ruta Chalepensis as Green Corrosion Inhibitor for Copper CDA 110 in 3% NaCl Medium: Experimental and Theoretical Studies

N. Ammouchi,[1,2] H. Allal,[2] E. Zouaoui,[2,*] K. Dob,[2] D. Zouied[2] and M. Bououdina[3]

[1]*Laboratory of Physico-Chemical research of Surfaces and Interfaces, University 20 Août 1955, Skikda, Algeria.*

[2]*Department of Technology, Faculty of Technology, 20 August 1955 University of Skikda, Algeria*

[3]*Department of Physics, College of Science, University of Bahrain, PO Box 32038, Kingdom of Bahrain*

*Corresponding Author, Tel.: +213775185200; Fax: +213770844152

E-Mail: zouaoui_amna@yahoo.fr

Received: 4 May 2019 / Received in revised form: 22 June 2019 /
Accepted: 3 July 2019 / Published online: xxxx 2019

Abstract- The corrosion inhibition of copper CDA 110 in 3% NaCl by Ruta Chalepensis' extract is studied by using electrochemical stationary and non-stationary methods. The obtained results reveal a significant enhancement of the inhibition efficiency by increasing the extract concentration. The adsorption behavior is found to obey Langmuir isotherm. Polarization study shows a cathodic character for the green leaves. The increase of medium temperature accelerates the corrosion process. The values of activation energy and thermodynamic parameters are calculated. In-depth the first principles calculations based on density functional density have been performed in order to evaluate the electronic structure and to understand the corrosion mechanism

Keywords- Corrosion inhibitor, Copper CDA 110, Plant extract, Electrochemical impedance spectroscopy, Density functional theory

1. INTRODUCTION

Corrosion is the most devastating and damaging phenomenon of modern technology and pose a serious threat to many industries. Several researches published yearly are devoted to corrosion and corrosion protection of different metals [1]. A number of organic compounds have been studied and employed as corrosion inhibitors [2]. The efficiency of these organic corrosion inhibitors is related to the presence of polar function containing S, O and N atoms which are centers for the established for the adsorption process [3]. However, because of their high cost and the growing awareness of health and ecological risks, we are looking for highly effective, cheaper and nontoxic inhibitors [4]. Bio-inhibitors application is an interesting methods of the protection against corrosion [5-7].

Plant extracts are natural organics containing different constituents including tannins, alkaloids, carbohydrates, proteins, pigments… which can limit corrosion on reactive sites of metal surface [8,9]. Many researchers have studied the use of natural substances to prevent corrosion of metals in acidic and alkaline environments such as Punicagranatum [10], Occimumviridis [11], Bamboo leaf [12] Extracts of henna [13,14], Oxandraasbeckii[15], Osmanthusfragran [16], lawsonia [17], Murrayakoenigii [18], Jasminumnudiflorum [19], Isertiacoccinea [20], Uncariagambir [21], Azadirachtaindica, Phyllanthusamarus [22], Oleaeuropaea [23], Nigella sativa [24]. Mejri et al. [25] studied the chemical composition of the essential oil of Rutachalepensis L, and reported that the 2-undecanone compound is the major component.

On the other hand, computational chemical calculations represent a very powerful tool for studying corrosion inhibition mechanism [26-28]. Soltani et al. [29] investigated the geometrical and electronic molecular structures of Salvia officinalis leaves extract on 304 stainless steel corrosion in 1 M HCl solution using computational methods. Quite recently, Allal et al. [30] have investigated the inhibition behavior of the thiophene derivatives as aluminum corrosion inhibitors, and investigated the relation between the inhibition efficiency and calculated quantum chemical parameters, such as highest occupied molecular orbital energy (E_{HOMO}), lowest unoccupied molecular orbital energy (E_{LUMO}), energy gap (ΔE_{Gap}), dipole moment (μ), polarizabilities $<\alpha>$, global hardness (η), global softness (σ) and global electrophilicity (ω).

Recently, we have studied the effect of curcuma and saffron on the corrosion protection of A106 Gr B carbon steel in 3% NaCl medium [31], as well as corrosion inhibition of Monel 400 with Mespilus japonica, Ricinus communis L and Vitisvinifera leaves extracts in hydrochloric solution [32]. In line with our previous studies, the present research work aims to investigate the corrosion inhibition efficiency of Ruta Chalepensis extracts as natural substance toward copper CDA 110 in NaCl 3% medium at various concentrations and temperature using electrochemical impedance spectroscopy and potentiodynamic polarization measurements. A theoretical study of two organic compounds, 2-Undecanone and 2-Dodecanone (first and

second major components of Ruta chalepensis L), has been performed using density functional theory (DFT).

2. EXPERIMENT PART

2.1. Materials

Copper specimens of dimensions 1×1×0.25 cm having the following chemical composition: 99.03 Cu, 0.03 Mn, 0.02 Fe, 0.12 Zn, 0.02 Pb, 0.03 Bi (in wt. %).

2.2. Preparation of the Working Electrode

The specimens were embedded in epoxy resin leaving a working area of 0.98 cm^2 in contact corrosive medium. The working surface was subsequently ground with 600 and 2400 grit grinding papers cleaned by distilled water then degreasing with acetone and rinsing with distilled water, followed by drying under air stream to avoid any kind of reaction between the distilled water and the polished surface before measurements.

2.3. Testing Environment

The corrosive medium is NaCl 3% was prepared by dissolving 30 g NaCl in 1000 ml of distilled water, and stirred to get a homogeneous solution.

2.4. Preparation of Plant Extract

RutaChalepensis was collected from Skikda region located at the north of Algeria in February 2017, then cleaned with water and air dried at room temperature. The plant extract are obtained according to the diagram illustrated in Figure 1.

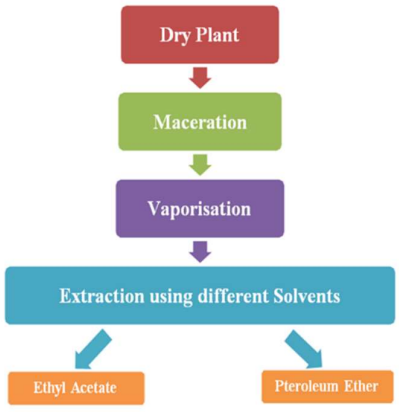

Fig. 1. The extraction of the plant *Electrochemical Measurements*

The polarization experiments and electrochemical impedance spectroscopy (EIS) were performed using a Voltalab PGZ 301 "All-in- one" Potentiostat/Galvanostat system. The potentials were measured against and referred to the saturated calomel electrode. The polarization experiments were carried out in the range of potential from (-1200) to (-200) mv using a scan rate of 10 mV/s. Measurements of impedance (Z) and phase shift were made in the range of 100 KHz to 100 mHz frequency [2c]. Q2

2.5. Computational Details

The studied compound was initially prepared and minimized by using Avogadro program [35] applying MMFF94s force field. The DFT quantum chemical calculations were performed with ORCA 4.0.1.2 computational package [36-37], under an open source code developed by Prof. Frank Neese. A geometry optimization of the studied compound (Table 1) was carried out in the aqueous phase involving CPCM models [38], using the CAM-B3LYP [39] functional and employing triple-ζ quality basis sets def2-TZVPP [40]. The atomic orbital integrals were calculated by the LIBINT library [40] and the natural population analysis (NPA) was performed with JANPA program (version 1.04) [41].

Table1. The name, molecular formula, molecular weight, molecular structure and number of atoms for studied inhibitor

Molecular name	Molecular formula	Molecular Weight (amu)	Molecular structure	Number of Atoms
2-Undecanone	$C_{11}H_{22}O$	170.292	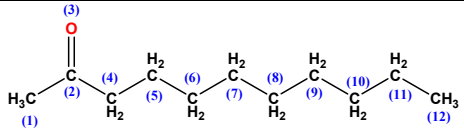	34

In order to evaluate our experimental results, we calculated the global reactivity descriptors like the energy of highest occupied molecular orbital (E_{HOMO}), energy of lowest unoccupied molecular orbital (E_{LUMO}), energy gap (ΔE_{Gap}), ionization potential (I), electron affinity (A), molecular volume for the van der Waals (V^{vdw}), surface-area (SA), dipole moment (μ), polarizability <α>, electronegativity (χ), chemical potential (π), global hardness (η), global softness (σ) and electrophilicity (ω).

$$I = -E_{HOMO} \quad (1)$$

$$A = -E_{LUMO} \quad (2)$$

$$\Delta E_{Gap} = E_{LUMO} - E_{HOMO} \quad (3)$$

$$\chi = -\pi = \frac{I+A}{2} \quad (4)$$

$$\eta = \frac{I-A}{2} \quad (5)$$

$$\sigma = \frac{2}{I-A} \quad (6)$$

$$\omega = \frac{\chi^2}{2\eta} \quad (7)$$

$$< \alpha > = \frac{1}{3}(\alpha_{xx} + \alpha_{yy} + \alpha_{zz}) \quad (8)$$

3. RESULTS AND DISCUSSION

3.1. Influence of Inhibitor Concentration

3.1.1. Potentiodynamic Polarization Measurement

Potentiodynamic polarization curves for copper in 3% NaCl medium in the absence and the presence of various concentration of Ruta Chalepensis are shown in Figures 2 and 3.

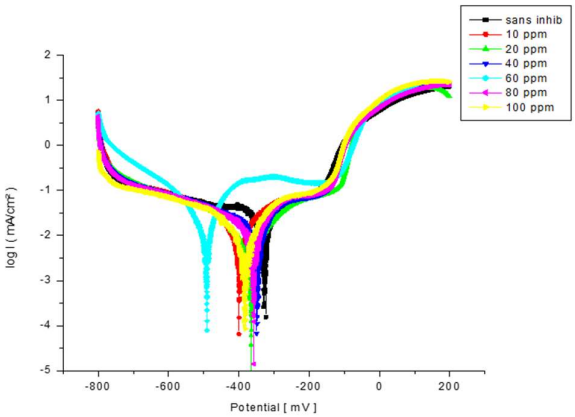

Fig. 2. Polarization curves of copper in 3% NaCl containing different concentration of Ruta Chalepensis leave (Extract 1)

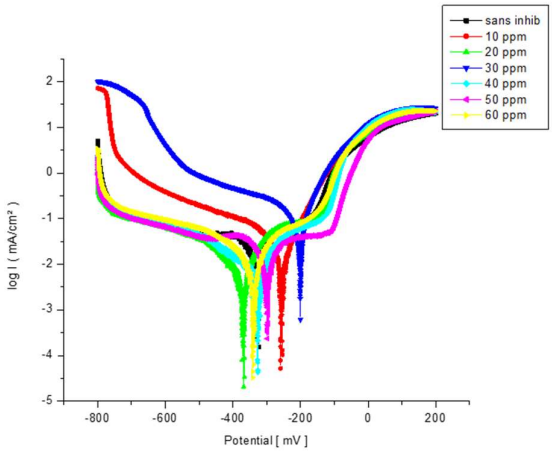

Fig. 3. Polarization curves of copper in 3% NaCl containing different concentration of Ruta Chalepensis leave (Extract 2)

The potentiodynamic polarization curves show a current plateau, which can be attributed to an oxygen diffusional control involved in the cathodic reaction [48-49], according to the reaction:

$$4H^+ + O_2 + 4e^- \rightarrow 2H_2O \quad (9)$$

The potentiodynamic polarization curves show a current plateau, which can be attributed to an oxygen diffusional control involved in the cathodic reaction [48-49], according to the reaction:

$$Cu^+ + Cl^- \rightarrow CuCl_{ads} \quad (10)$$

Moreover, for the curve corresponding to 40 ppm, optimal concentration for the extract 1, there is a disappearance of the passivation level in the cathodic branch, whereas in the anode branch there has been an increase in the plateau.

The electrochemical parameters such as corrosion potential (E_{corr}), corrosion current (I_{corr}), cathodic and anodic Tafel slopes and inhibitor efficiencies are given in Table 2.

Table 2. Electrochemical parameters for copper in 3% NaCl solution in the presence and absence of inhibitor

C $_{inhib}$ (ppm)	**$E_{(I=0)}$ (mV)**	**Rp (ohm.cm^2)**	**i_{corr} (mA/cm^2)**	**B_a (mV)**	**B_c (mV)**	**E (%)**
00 ppm	-328,7	117,68	0,1398	202	-449,5	-
Extract 1						
10 ppm	-398.4	1370	0.0397	175.2	-526.6	71.60
20 ppm	-365	955.22	0.0380	158.1	-424 ;8	72.81
40 ppm	-491.9	4800	0.0197	98.4	-150.7	85.90
60 ppm	-356	2530	0.0253	166.7	-489.7	81.90
80 ppm	-385.3	1050	0.0294	152.9	-572 .8	78.96
Extract 2						
10 ppm	-254.1	337.85	0.0395	111.9	-342.8	71.74
20 ppm	-368.2	366.09	0.0290	175.1	-543.1	79.25
40 ppm	-329 .2	532.9	0.0170	93.1	-417.4	87.83
50 ppm	-298.6	566.63	0.0166	95.7	-487.8	88.12
60 ppm	-341.7	500	0.0190	107	-446	86.40

The analysis of the polarization curves (Figures 2 and 3) and the results in Table 2 show that the current density (I_{corr}) decreases with the increase of the inhibitor concentration from 10 to 40 ppm (the optimum value for extract 1) and 50 ppm (the optimum value for extract 2). The polarization resistance reaches maximum values of 1960 and 566 (Ω.cm2) for the concentration 40 and 50 ppm respectively.

It is reported in the literature that, depending on the value of the displacement of E_{corr} in the presence of the inhibitor, the inhibitor is considered as (i) anodic or cathodic for E_{corr} greater than ±85 mV/SCE relative to E_{corr} of the blank and (ii) mixed inhibitor for E_{corr} less than ±85 mV/SCE [15-16]. In the case of extract 1, the variation of E_{corr} is found to be greater than ±85 mV/SCE; for all concentrations the potential is shifted to negative values which implies that this extract acts as a cathodic inhibitor. Whereas for extract 2, E_{corr} is less than ±85 mV/SCE, which confirms the mixed character of the inhibitor. It reduces the anodic dissolution of copper described by the reaction ($Cu \leftrightarrow Cu^{+} + e^{-}$) meanwhile delays the cathodic reaction. The decrease of I_{corr} and the increase of R_p is mainly due to the reduction of the Cl^- attack on the surface of copper which causes the decrease of its dissolution by the adsorption of the inhibitor molecules [50].

The higher values of the polarization resistance (1960 and 566.63 $\Omega.cm^2$) with the lowest current density values (2.54 and 5.172 mA/cm^2) correspond to the optimal concentrations of extrats 1 and 2, respectively (40 and 50 ppm).

It can be noticed that the effectiveness of each inhibitor rises with the increase in its concentrations and reaches maximum values of 85.90% for 40 ppm of extract 1 and 88.12% for 50 ppm of extract 2.

3.2. Electrochemical Impedance Measurements

Electrochemical impedance measurements gives important information on mechanisms and reaction kinetics for a metal/electrolyte electrochemical system [51-52]. It allows to identify by their relaxation time the different processes taking place at the metal/electrolyte interface. Fast processes usually occur at high frequencies. When the applied frequency decreases, the contribution of the slower steps, such as transport or diffusion phenomena in solution, appears [53].

The impedance spectra recorded at room temperature without and with various concentrations of the inhibitor in NaCl 3% solution are shown in Figures 4 and 5.

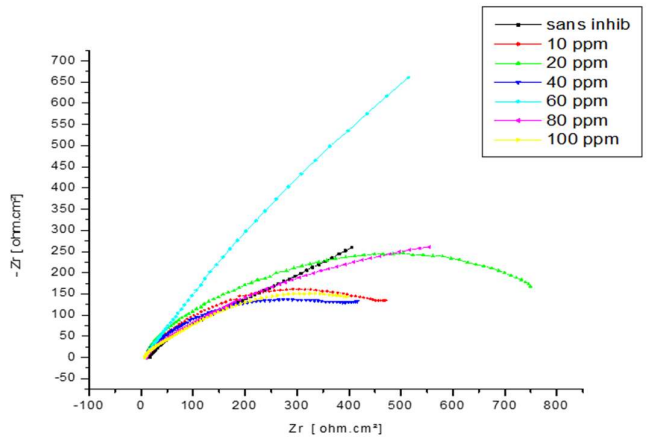

Fig. 4. Nyquist plots for copper in a 3% NaCl solutions without and with different concentrations of extract 1 Q3

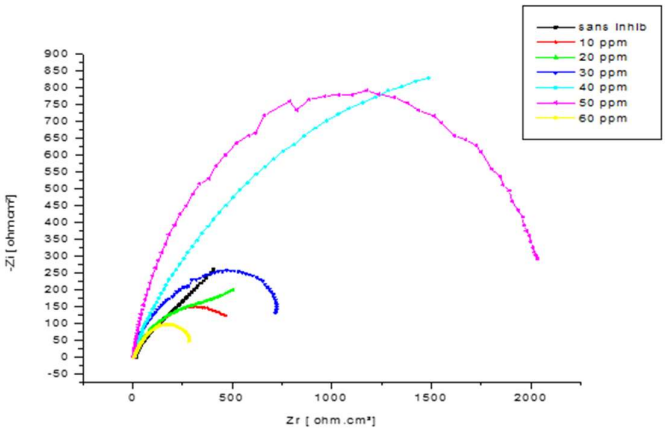

Fig. 5. Nyquist plots for copper in a 3% NaCl solutions without and with different concentrations of extract 2 Q3

Nyquist plots are often used in the electrochemical literature because they allow for an easy calculation of the impedance corrosion elements [54]. The values of the solution resistance (R_s), the charge transfer resistance (R_{tc}) and the total capacitance (Q) were calculated by simulating the experimental data with the EC-Lab software. The results are listed in Table 3.

Table 3. Inhibitory efficiencies and electrochemical parameters deduced from the impedance diagrams in the absence and in the presence of inhibitors at different concentrations

C_{inhib} (ppm)	R_s (Ohm)	Q ($F.S^{(a-1)}$)	a	R_{tc} (Ohm)	S ($Ohm.S^{-1/2}$)	E (%)
00 ppm	15,53	0,340 $7e^{-3}$	0,7034	149,8	316,5	-
Extract 1						
10 ppm	8.887	0.192 $4e^{-3}$	0.7319	1096	-	86.33
20 ppm	7.314	0.208 $4e^{-3}$	0.6975	754.3	-	80.14
40 ppm	7.224	0.373 $8e^{-3}$	0.689	2495	-	93.99
60 ppm	8.052	0.807 $8e^{-3}$	0.5681	777.1	-	80.72
Extract 2	7.87	0.352 $2e^{-3}$	0.6474	493.8	-	69.66
10 ppm						
20 ppm	5.234	0.414 $7e^{-3}$	0.6405	517.8	-	71.06
40 ppm	6.034	0.334 $7e^{-3}$	0.7424	1932	-	92.24
50 ppm	6.072	39.77 e^{-6}	0.8696	2001	-	92.51
60 ppm	6.998	0.514 $7e^{-3}$	0.6388	436.2	-	65.65

The Nyquist plots show the existence of a single capacitive loop, which indicates that the dissolution process is controlled by the charge transfer reaction [55]. The loop size increases gradually with increasing inhibitor concentration while its shape is similar for all the concentrations, which indicates that there is no change in the corrosion mechanism [56]. Moreover, it can be observed that the loops are not perfect semicircles that can be attributed to frequency dispersion due to non-roughness and heterogeneity of the electrode surface [57].

The results obtained show that there is an increase of the R_{tc} with the increase of the inhibitor concentration and reaches a maximum value at 40 ppm for the extract 1 and 50 ppm for the extract 2, while the values of the C_{dc} decrease, because the addition of inhibitor increases the adsorption over the metal surface by forming a protective layer. Thus, the electron transfer between the metal surface and the corrosive medium decreases [58]. An equivalent circuit for such an electrode can be used to model the corrosion process, as shown in Figure 6.

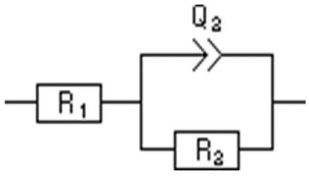

Fig. 6. Equivalent for Copper CDA 110 (a) in blank and (b) with inhibitor

3.3. Adsorption Isotherms

The effectiveness of a corrosion inhibitor depends mainly on its adsorption capacity at the metal/solution interface. It is often a displacement reaction involving the replacement of water molecules adsorbed on the metal surface by the inhibitor molecules [59]. Generally, adsorption is described by physical and/or chemical adsorption. Therefore, it is essential to know the mode of adsorption that can give information on the inhibitor interaction on the metal surface. To better describe the adsorption of Ruta Chalepensis leaves on copper surface, different adsorption isotherms are used [60]; (i) Temkin (eq. 11); (ii) Langmuir (eq. 12) and (iii) Frumkin (eq. 13) given by the following equations:

$$C.K_{ads} = exp(-2a\theta) \quad (11)$$

$$C/\theta = 1/K_{ads} + C \quad (12)$$

$$C.K_{ads} = \theta/(1-\theta)exp^{f0}(2a\theta) \quad (13)$$

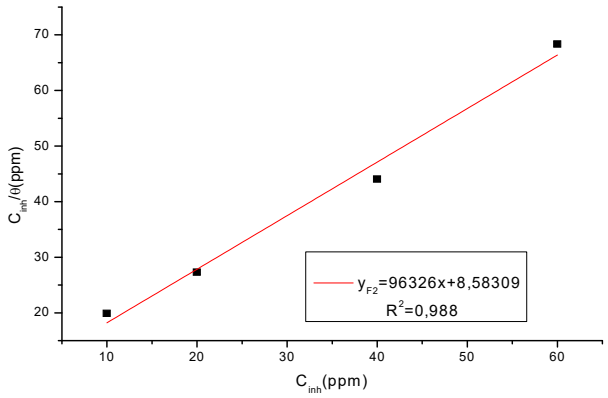

Fig. 7. The Langmuir adsorption isotherm for extract 1

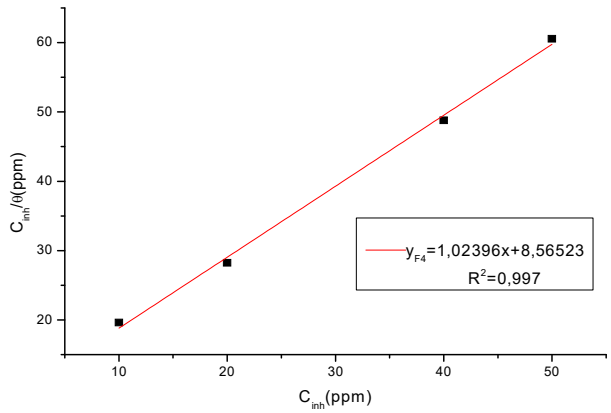

Fig. 8. The Langmuir adsorption isotherm for extract 2

The adsorption isotherms shown in the Figures 7 and 8 indicate that the Langmuir model is the most suitable isotherm, it assumes the existence of a determined number of adsorption sites and each site can only accommodate one adsorbed species. Moreover, no interactions between the adsorbed particles occurs and the adsorption energy is considered constant and therefore, the inhibition is due to the formation of a monolayer on the surface of the metal limiting the access of the electrolyte [61].

The values of the adsorption equilibrium constants are obtained from the intersection between C_{inh}/Θ and C_{inh} . To calculate the values of adsorption energies, the following equation is used: ΔG °ads =-R.T. ln(55.5 K_{ads}) where R is the perfect gas constant (8.314 J/K.mol), T is the absolute temperature (293 °K) . The values of K_{ads} and $\Delta G°$ ads are presented in Table 4.

Table 4. The different values of the Kads constant and the adsorption energy deduced from the Langmuir isotherm for the two extracts

	L'équation	R^2	K_{ads}	$\Delta G°_{ads}$(Kj/mol)
Extract 1	Y=1.02396x+8.588309	0,988	0,11650816	-4.624
Extract 2	Y=1.02396x+8.56523	0,997	0,1167511	-4.629

The thermodynamic adsorption parameters can provide information on the mechanism of corrosion inhibition; a negative value of $\Delta G°_{ads}$ indicates a spontaneous adsorption process and the stability of the adsorbed layer on metal surface. Generally, the values of $\Delta G°_{ads}$ are around -20 kJ.mol^{-1} and represent an electrostatic interaction between charged metal surface and the charged molecules (physisorption). Meanwhile, negative values of more than -40 kJ.mol^{-1} involve the sharing or transfer of electrons from inhibitor molecules to the metal surface to form a coordination type of bond (chemisorption) [62]. In our case, the values of $\Delta G°$ ads are smaller; -4.6 and -4.6 kJ/mol for extracts 1 and 2 respectively, there by indicating a physisorption mechanism.

3.4. Effect of Temperature

3.4.1. Polarization Curve

The effect of temperature at optimum concentration has been studied by polarization measurement in the temperature range of 298-333 °K. The polarization curves of copper in 3% NaCl medium, without and with the inhibitor for the optimal concentration of extract 1 (40

ppm) and extract 2 (50 ppm) at different temperatures, are illustrated in Figure 9 and the corresponding electrochemical parameters are summarized in Table 5.

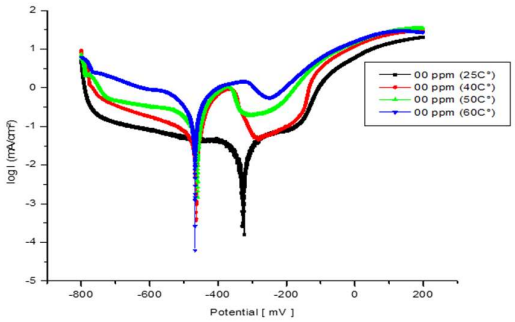

(a)

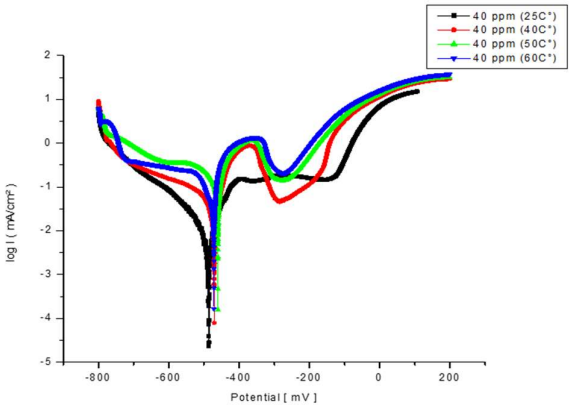

(b)

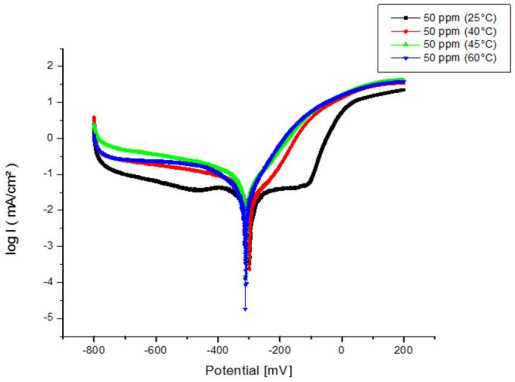

(c)

Fig. 9. Potentiodynamic polarization curves for the corrosion of copper CD 110 in 3% NaCl solutions at various temperatures (a) without inhibitor; (b) with 40 ppm of extract 1; (c) with 50 ppm of extract 2

Table 5. Electrochemical polarization parameters for the corrosion of copper CD 110 in 3% NaCl solutions containing inhibitor at different temperatures

Température (°C)	$E_{(I=0)}$ (mV)	R_p (ohm.cm^2)	i_{corr} (mA/cm^2)	B_a (mV)	B_c (mV)
Blank					
25	-328 ,7	117,68	0,1398	202	-449,5
40	-463,2	123,04	0,1483	227,1	-445,5
50	-459,7	84	0,2075	263,6	-695,8
60	-467,5	85,60	0,2986	271,4	-302,9
Extract 1					
25	-486.4	1960	0.0187	106	-177.1
40	-470 .6	1170	0.0546	177	-230.6
50	-471.3	204.18	0.0754	224	-288
60	-459.8	112.27	0.1048	247.9	-337.7
Extract 2					
25	-298.6	566.63	0.0166	95.7	-487.8
40	-300.5	139.92	0.0798	82.1	-824.4
50	-309.4	49.21	0.1316	97	-690.2
60	-312.6	48.72	0.1616	92.4	-1774.8

According to the polarization results, it can be concluded that increasing the temperature from 298 to 333K causes:

-An increase in the value of the density of the corrosion current,

-A decrease in the polarization resistance,

-The inhibitory efficiency decreases considerably with the increase in temperature showing a significant desorption phenomenon [62].

3.5. Thermodynamic Parameters

The values of the activation energy E_a, activation enthalpy ΔH_a, activation entropy ΔS_a can be determined from the following equations:

$$I_{corr} = \frac{RT}{Nh} exp\left(\frac{\Delta S^{\circ}}{R}\right) exp\left(-\frac{\Delta H^{\circ}}{R}\right) \quad (14)$$

$$I_{corr} = Kexp\left(-\frac{E_a}{R\,T}\right) \quad (15)$$

where I_{corr} is the corrosion current density ($A.cm^{-2}$), L is a constant, E_a is the activation energy ($kJ.mol^{-1}$), R is the perfect gas constant ($J.mol^{-1}.K^{-1}$), T the temperature, h: Plank constant, N: Avogadro number, ΔH_a: Activation enthalpy and ΔS_a: Activation entropy.

The apparent activation energy can be determined from the slope of $\ln(I_{corr})$ *vs.* 1/T graph, as shown in Figure 12(a), whereas ΔH_a and ΔS_a are obtained from the slope of (-ΘHa/R) and interception of ($\ln R/Nh+\Delta S_a/R$) as shown in Figure 12(b), and the corresponding values are summarized in Table 4. Figure 10 illustrates the variation of $\ln(I_{corr})$and $\ln(I_{corr}/T)$ *vs* of 1/T for copper in 3% NaCl solution.

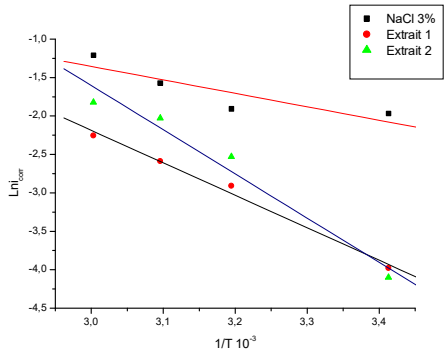

(a)

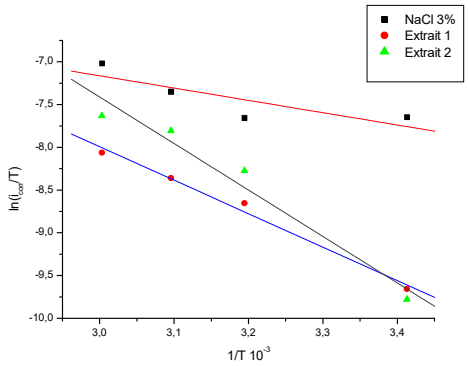

(b)

Fig. 10. Relationship between temperature and current density in 3% NaCl solution

Table 6. Thermodynamic activation parameters of copper in the absence and presence of extracts in 3% NaCl solution obtained from electrochemical measurements

	$E°_a$ (KJ/mol)	$\Delta H°_a$ (KJ/mol)	$\Delta S°_a$ (J/mol)
NaCl 3%	14,561	11,974	-65,073
Extract 1	35,113	32,511	-10,220
Extract 2	47,811	45,225	32,615

From the results obtained in Table 6, it can be concluded that:

-The inhibitors are adsorbed on the surface through bonds of electrostatic nature (physisorbed on the surface of the electrode). Indeed, the E_a values for the 2 extracts are greater than the value of E_a obtained for the solution without inhibitor.

-The positive sign of enthalpy reflects the endothermic nature of the copper dissolution process. In fact, the increase of the activation enthalpy corresponds to a decrease in the dissolution of the metal.

-The negative value of the entropy means that there is a decrease in the disorder during the transformation of the reagents into an activated Cu-molecule complex in the solution, whereas the positive value corresponding to the extract 2 implies an increase in the disorder. This increase in entropy may be caused by the imperceptible replacement of water molecules due to the adsorption of inhibitor molecules on the metal.

3.6. Computational Chemical Calculations

The frontier orbital (highest occupied molecular orbital HOMO and lowest unoccupied molecular orbital LUMO) have been used in order to predict adsorption centers of the inhibitor compounds. From HOMO and LUMO orbitals illustrated in Figure 11, it can be concluded that both HOMO and LUMO are mainly localized around the carbonyl group, with a contributions of 68% for HOMO and 77% to the LUMO.

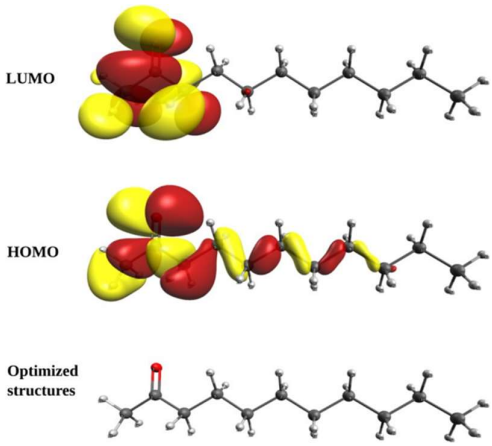

Fig. 11. Optimized structures, HOMO and LUMO of the optimized studied inhibitor**,** obtained at CAM-B3LYP/def2-TZVPP level

The selected parameters (bond length (Å), bond angles (°), dihedral angles (°)) of the studied compounds are summarized in Table 7. The calculated bond length of carbonyl group (C═O) is 1.214 Å, smaller than the calculated bond length of C═O for 2-propanone (or acetone) [63].

Table 7. Bond lengths (Å), bond angles (°) and dihedral angles (°) of the optimized studied inhibitor, obtained at CAM-B3LYP/def2-TZVPP level

Bond lengths (Å)		Bond angles (°)		Dihedral angles (°)	
C2—C1	1.5008	**O3—C2—C4**	122.18	**C5—C4—C2—O3**	-9.44
O3—C2	1.2142	**C1—C2—O3**	121.35	**C5—C4—C2—C1**	172.19
C4—C2	1.5038	**C1—C2—C4**	116.49	**C6—C5—C4—C2**	179.34
C5—C4	1.5167	**C2—C4—C5**	115.31	**C7—C6—C5—C4**	179.47
C6—C5	1.5221	**C4—C5—C6**	112.49	**C8—C7—C6—C5**	179.93
C7—C6	1.5216	**C5—C6—C7**	113.29	**C9—C8—C7—C6**	179.77
C8—C7	1.5218	**C6—C7—C8**	113.44	**C10—C9—C8—C7**	-181.91
C9—C8	1.5219	**C7—C8—C9**	113.55	**C12—C11—C10—C9**	-181.85
C10—C9	1.5217	**C8—C9—C10**	113.54		
C11—C10	1.5221	**C9—C10—C11**	113.58		
C12—C11	1.5215	**C10—C11—C12**	113.9		

The natural population analysis (NPA) has been calculated in order to provide a quantitative description of the electron density redistribution. From Table 8, it can be concluded that the (O3) atom carry negative charged centers, and consequently, suggesting that the most favorable site for electrophilic attack.

Table 8. Calculated atomic charges (obtained from NPA method)of the optimized studied inhibitor, obtained at CAM-B3LYP/def2-TZVPP level

Atoms	NPA
C1	-0.7190
C2	0.6303
O3	-0.6177
C4	-0.5065
C5	-0.3848
C6	-0.3801
C7	-0.3804
C8	-0.3802
C9	-0.3808
C10	-0.3828
C11	-0.3841
C12	-0.5997

In addition, the weak interactions are studied by employing the NCI (Non-Covalent Interaction) approaches [64]. For that reason, the electrostatic potential (ESP) and reduced density gradient (RDG) analysis implemented in Multiwfn 3.3.9 package [65] are used. The ESP and RDG maps are plotted respectively in Figures 14 and 15, generated using by VMD software [66]. It should be noted that the two 3D-NCI plots ESP and RDG provides information on the reactivity of the molecules with electrophiles or nucleophiles.

In Figure 12, the ESP values are in the range -48.6 -26.4 kcal/mol. However, the red and blue colors represent the positive diffusion region and the negative diffusion region, respectively. The negative ESP regions distribute over the oxygen atom (O3) of carbonyl group which possess the global minimum (−48.59 kCal/mol), and thus reveals the most susceptible sites for electrophilic attack, and consequently the favorite sites for interaction with the metal surface. On the other hand, from the reduced density gradient (RDG) iso-surfaces shown in Figure 13, the interaction region marked by green between C2=O3•••H19 atoms, can be determined as Van der Walls interaction region.

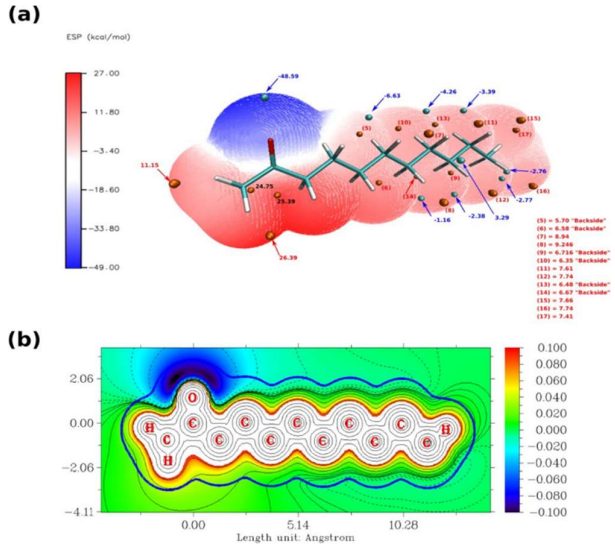

Fig. 12. Plots of Electrostatic Potential (ESP) on the Van der Waals surface: (a) 3D-ESP plots; (b) 2D- ESP map

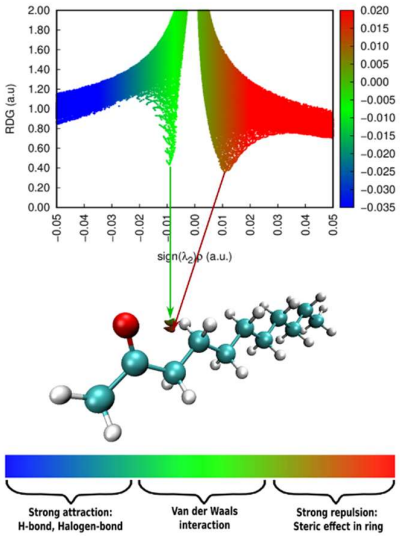

Fig. 13. Color-filled reduced density gradient (RDG) map

Table 9. Calculated quantum chemical parameters (a) for the neutral forms of the studied compounds

Parameters	**2-Undecanone**	**2-Dodecanone**
$\mathbf{E_{HOMO}}$ (eV)	-8.778	-8.777
$\mathbf{E_{LUMO}}$ (eV)	0.919	0.918
$\mathbf{\Delta E_{Gap}}$ (eV)	9.696	9.695
I (eV)	8.778	8.777
A (eV)	-0.919	-0.918
TE (a.u.)	-507.583	-546.887
μ (Debye)	4.121	4.234
< α > (a.u.)	181.964	198.323
$\mathbf{V^{vdw}}$ ($Bohr^3$)	897.786	972.631
SA ($Bohr^2$)	501.632	540.191
χ	3.929	3.93
π	-3.929	-3.93
η	4.848	4.847
σ	0.206	0.206
ω	1.592	1.593

The calculated global descriptors of 2-Undecanone and 2-Dodecanone inhibitors (the first and second major components of Ruta chalepensis L) are listed in Table 9. It should be noted from Table 9 that the 2-Undecanone and 2-Dodecanone inhibitors have very close values of

parameters such as EHOMO, ELUMO, ΔE_{gap}, χ, η and ω. This means probably that both compounds have a similar behavior, certainly because their electronic structures have the same stereochemistry. However, the obtained results of global descriptors (listed in Table 9), should be useful for future studies that wish to examine and compare our molecular structures with their analogous, i.e. the acetone derivatives.

4. CONCLUSION

Q4

In this research work, the inhibiting effect of Ruta Chalepensis leaves on copper in 3% NaCl medium has been investigated experimentally and theoretically. The measurements have been carried out by non-stationary and stationary electrochemical methods with the variation of concentrations and temperature. From the obtained results, the following conclusions can be drawn:

-The electrochemical tests have shown that the extract 1 is a cathodic inhibitor and that the extract 2 is a mixed inhibitor.

-The inhibitory efficiency increases with increasing extracts' concentration and reaches a maximum value of 87.80% for 40 ppm in the presence of the extract1 and 82.61% in the presence of inhibitor of extract 2 for 50 ppm.

-The increase in temperature of the medium decreases the protective power of the inhibitor and increases the corrosion current.

-The adsorption of Ruta Chalepensis leaves can be approximated by the Langmuir adsorption isotherm.

-The negative value of ΔG_{ads} indicates that the adsorption process is spontaneous.

REFERENCES

[1] I. Radojcic, K. Berkovic, S. Kovac, and J. Vorkapic'-Furac, Corros. Sci. 50 (2008) 1498.

[2] E. Zouaoui, F. Krid, S. Kharraf, and M. S. Medjram, Algerian J. Natural Product. 2 (2014) 105.

[3] I. B. has Obot, S. A. Umoren, and N. O. Obi-Egbedi, J. Mater. About. Sci. 2 (2011) 60.

[4] S. Khoudali, D. Benmessaoud, A. Essaqui, M. Zertoubi, M. Azzi, and M. Benaissa, J. Mater. About. Sci. 5 (2014) 887.

Q5

[5] L. Valek, S. Martinez, D. Mikulic, and I. Brnardic, Corr. Sci. 50 (2008) 2705.

[6] J. S. Chauhan, Asian J. Chem. 21 (2009) 1975.

[7] H. I. Farooqi, M. A. Quraishi, and P. A. Saini, Proceed. Europ. Federat. Corros. I (1997) 186.

[8] M. Mishra, K. Tiwari, A. Kumar Singh, and V. P. Singh, Polyhedron 77 (2014) 57.

[9] D. Q. Zhang, Q. R. Cai, L. X. Gao, and K. Y. Lee, Corr. Sci. 50 (2008) 3615.

[10] D. Q. Zhang, L. X. Gao, and J. D. Zhou, J. Appl. Surf. Sci. 225 (2004) 287.

[11] T. Poornima, J. Nayak, and A. N. Shetty, Corr. Sci. 53 (2011) 3688
[12] S. Banerjee, V. Shrivatsava, and M. M. Singh, Corr. Sci. 59 (2012) 35
[13] S. Martinez, L. Valek, and I. S. Oslakovic, J. Electrochem. Soc. 154 (2007) 671
[14] S. M. Park, and J. S. Yoo. Anal. Chem. 75 (2003) 488A
[15] S. M. Park, J. S. Yoo, and E. S. Ahn, Pure. Appl. Chem. 78 (2006) 1069
[16] A. Dieter, Corrosion et Chimie de Surface des Métaux, 1 ère Edition, Presses Polytechniques et Universitaires Romandes CH-1015 Lausanne (1993) 553 pages.
[17] X. Joseph Raj, and N. Rajendran, Int. J. Electrochem. Sci. 6 (2011) 348.
[18] W. Li, L. Hu, S. Zhang, and B. Hou, Corr. Sci. 53 (2011) 735.
[19] E. Hamed, S. Abd El-Rehim, M. F. El- Shahat, and A. M. Shaltot, Mater. Sci. 177 (2012) 441.
[20] D. Hmamou, R. Ben. Salghi, A. Zarrouk, H. Zarrok, R. Touzani, B. Hammouti, and El Assyry, J. Environ. Chem. Eng. 3 (2015) 2031.
[21] A.O. Yuce, B.D. Mert, G. Kardas, B. Yazici, Corr. Sci. 83 (2014) 310
[22] a) K. F. Khaled, and N. Hackerman, Electrochim. Acta 49 (2004) 485.
b) S. El-Issami, L. Bazzi, M. Hilali, R. Salghi, and S. Kertit, Ann. Chim. Sci. Mater. 27 (2002) 63.
[23] M. Scendo. Corros. Sci. 47 (2005) 2778.
[24] M. Gopiraman, P. Sakunthala, D. Kesavan, V. Alexramani, I. S. Kim, and N. J. Sulochana, Coat. Technol. Res. 9 (2012) 15.
[25] J. Mejri, M. Abderrabba, and M. Mejri, Industrial Crops and Products 32 (2010) 671.
[26] A. Zarrouk, H. Zarrok, R. Salghi, B. Hammouti, S. S. Al-Deyab, R. Touzani, M. Bouachrine, I. Warad, and T. Ben Hadda, Int. J. Electrochem. Sci. 7 (2012) 6353.
[27] G. Gece, Corros. Sci. 50 (2008) 2981.
[28] N. O. Obi-Egbedi, I. B. Obot, and M. I. El-Khaiary, J. Mol. Struct. 1002 (2011) 86.
[29] N. Soltani, N. Tavakkoli, M. Khayatkashani, M. R. Jalali, and A. Mosavizade, Corros. Sci. 62 (2012) 122.
[30] H. Allal, Y. Belhocine, and E. Zouaoui, J. Mol. Liquids 265 (2018) 668.
[31] K. Dob, E. Zouaoui, and D. Zouied, Anti-corrosion Method. Mater. 65 (2018) 225.
[32] S. Kharref, E. Zouaoui, and M. S. Medjram. Anti-corrosion Method. Mater. 64 (2017).
[33] A. D. Becke, J. Chem. Phys. 98 (1993) 5648.
[34] A. D. Becke, J. Chem. Phys. 84 (1986) 4524.
[35] M. D. Hanwell, D. E. Curtis, D. C. Lonie, T. Vandermeersch, E. Zurek, and G. R. Hutchison, J. Cheminform 4 (2012) 1.
[36] F. Neese, The ORCA program system, Wiley Interdiscip. Rev. Comput. Mol. Sci. 2 (2012) 73.
[37] F. Neese, Software update: the ORCA program system, version 4.0, Wiley Interdiscip. Rev. Comput. Mol. Sci. 8 (2018) e1327.

[38] V. Barone, and M. Cossi, J. Phys. Chem. A 102 (1998) 1995.
[39] T. Yanai, D. P. Tew, and N. C. Handy, Chem. Phys. Lett. 393 (2004) 51.
[40] F. Weigend, and R. Ahlrichs, Phys. Chem. Chem. Phys. 7 (2005) 3297.
[41] T. Y. Nikolaienko, L. A. Bulavin, and D. M. Hovorun, Theor. Chem. 1050 (2014) 15.
[42] T. Koopmans, Physica 1 (1934) 104.
[43] P. Geerlings, F. De Proft, and W. Langenaeker, Chem. Rev. 103 (2003) 1793.
[44] W. Yang, and W. J. Mortier, J. Am. Chem. Soc. 108 (1986) 5708.
[45] W. Yang, and R. G. Parr, Proc. Natl. Acad. Sci. 82 (1985) 6723.
[46] P. K. Chattaraj, B. Maiti, and U. Sarkar, J. Phys. Chem. A 107 (2003) 4973.
[47] P. Fuentealba, and O. Reyes, J. Mol. Struct. Theochem. 282 (1993) 65.
[48] J. Hu, D. Huang, G.L. Song and X. Guo, Corros. Sci. 53 (2011) 4093.
[49] P. Thanapackiam, Anti-Corrosion method. Mater. 64 (2017) 92.
[50] P. Mourya, S. Banerjee, and M. M.Singh, Corros. Sci. 85 (2014) 352.
[51] L. Feng, H. Yang, and F. Wang, Electrochim. Acta 58 (2011) 427.
[52] A. A. Al-Amiery, A. A. H. Kadhum, A. B .Mohamad, and S. A. Junaedi, Materials 6 (2013) 1420.
[53] P. Singh, E. E. Ebenso, L. O. Olasunkanmi, I. B. Obot, and M. A. Quraishi, J. Phys. Chem. C 120 (2016) 3408.
[54] M. Bouklah, B. Hammouti, M. Lagrenée, and F. Bentiss, Corros. Sci. 48 (2006) 2831.
[55] H. Ashassi-Sorkhabi, B. Shaabani, and D. Seifzadeh, Appl. Surf. Sci. 239 (2005) 154.
[56] E. S. S. R. A. Popova, Corros. Sci. 45 (2003) 33.
[57] M. A. Amin, G. A. M. Mersal, and Q. Mohsen, Arabian J. Chem. 4 (2011) 223.
[58] F. Bentiss, M. Lebrini, and M. Legrenee, Corros. Sci. 47 (2005) 2915.
[59] Y. I. Kuznetsov, Prot. Met. 37 (2001) 101.
[60] S. D. Deng, X. H. Li, and H. Fu, Corros. Sci. 53 (2011) 760.
[61] E. Cano, J. L. Polo, A. La Iglesia, and J. M. Bastidas, Adsorption 10 (2004) 219.
[62] A. M. Badiea, K. N. Mohana, Corros. Sci. 51 (2009) 2231.
[63] W. Koch, and H. Schwarz, Chem. Phys. Lett. 113 (1985) 145.
[64] E. R. Johnson, S. Keinan, P. Mori-Sánchez, J. Contreras-García, A. J. Cohen, and W. Yang, J. Am. Chem. Soc. 132 (2010) 6498.
[65] T. Lu, and F. Chen, J. Comput. Chem. 33 (2012) 580.
[66] W. Humphrey, A. Dalke, and K. Schulten, J. Mol. Graphics 14 (1996) 33.